Swinburne Research Bank
http://researchbank.swinburne.edu.au

Caulton, A.; Forbes, Duncan A.; Georgakakis, Antonis; Hopkins, A. M.; Wiklind, T. (2001). Cold gas in elliptical galaxies. *Monthly notices of the Royal Astronomical Society*. 326, (4): 1431-1440.
Available at: http://dx.doi.org/10.1046/j.1365-8711.2001.04677.x

© 2001 The Royal Astronomical Society.

This is the author's version of the work. It is posted here with the permission of the publisher for your personal use. No further distribution is permitted. If your library has a subscription to this journal, you may also be able to access the published version via the library catalogue.

The definitive version is available at www.interscience.wiley.com

Mon. Not. R. Astron. Soc. **000**, 000–000 (0000) Printed 1 February 2008 (MN LaTeX style file v1.4)

Cold gas in elliptical galaxies

A. Georgakakis[1⋆], A. M. Hopkins[2], A. Caulton[1], T. Wiklind[3], A. I. Terlevich[1], Duncan A. Forbes[4]

[1] *School of Physics and Astronomy, University of Birmingham, Edgbaston, Birmingham, B15 2TT, UK*
[2] *Department of Physics and Astronomy, University of Pittsburgh, 3941 O'Hara Street, PA 15260, USA*
[3] *Onsala Space Observatory, S-43992, Onsala, Sweden*
[4] *Astrophysics & Supercomputing, Swinburne University, Hawthorn, VIC 3122, Australia*

arXiv:astro-ph/0105435v1 24 May 2001

1 February 2008

ABSTRACT

We explore the evolution of the cold gas (molecular and neutral hydrogen) of elliptical galaxies and merger remnants ordered into a time sequence on the basis of spectroscopic age estimates. We find that the fraction of cold gas in early merger remnants decreases significantly for ≈1–2 Gyr, but subsequent evolution toward evolved elliptical systems sees very little change. This trend can be attributed to an initial gas depletion by strong star-formation which subsequently declines to quiescent rates. This explanation is consistent with the merger picture for the formation of elliptical galaxies. We also explore the relation between H I–to–H_2 mass ratio and spectroscopic galaxy age, but find no evidence for a statistically significant trend. This suggests little net H I to H_2 conversion for the systems in the present sample.

Key words: Galaxies: mergers – galaxies: starburst – radio continuum: galaxies

1 INTRODUCTION

One of the proposed mechanisms for the formation of elliptical galaxies is the "merger hypothesis" postulating that these systems are the product of disc galaxy mergers (Toomre & Toomre 1972). A number of studies suggest that although merger remnants have many properties that are different to those of ellipticals they will eventually evolve to resemble these systems. Several aspects of this evolution are briefly discussed by Georgakakis, Forbes & Norris (2000; Paper I). In particular, investigation of post-mergers at different evolutionary stages suggests that global properties such as star-formation, optical/far-infrared colours, and X-ray luminosity, evolve with time to values typical of old ellipticals (Casoli et al. 1991; Keel & Wu 1995; Georgakakis, Forbes & Norris 2000; O'Sullivan, Forbes & Ponman 2000a).

The "merger hypothesis" also faces some serious difficulties. One of the long standing problems of this scenario is the excess globular clusters (GCs) per unit starlight around ellipticals compared to spirals (van den Bergh 1984). Although evidence is accumulating that new GCs are formed during interactions (Whitmore & Schweizer 1995; Schweizer 1996; Miller et al. 1997; Zepf et al. 1999), it is still unclear whether these objects will evolve into *bona-fide* GCs (Brodie et al. 1998). Moreover, the properties of the GC population of many old ellipticals, when studied in detail, appear to be inconsistent with the merger scenario, suggesting that not all ellipticals form by mergers (Forbes et al. 1997).

Another challenge for the merger picture comes from the properties of cold gas in post-merger systems. In particular, the evolution of cold gas (H I and H_2) was investigated in Paper I along an age sequence comprising both pre- and post-mergers. A clear decrease can be seen in cold gas content with age after the merger event, but even the most advanced merger remnants in the sample (at "age parameters" of ≈ 1.5 Gyr) are still richer in cold gas than evolved ellipticals by about an order of magnitude. A number of mechanisms have been proposed that may account for this discrepancy, including gas depletion by residual star-formation activity, and gas heating to X-ray temperatures. Evidence exists that suggests such processes do occur in merger remnants (e.g. Hibbard & van Gorkom 1996), but it remains unclear whether there is a true evolutionary link between the cold gas properties of post-mergers and "normal" ellipticals. The merger remnants investigated in Paper I, however, were limited to "age parameters" (ages relative to the merger event) in the range 0.1–1.5 Gyr, and allow no conclusions to be drawn about cold gas evolution at later stages. This paper investigates these questions by extending the merger remnant sample of Paper I to include ellipti-

⋆ age@star.sr.bham.ac.uk

© 0000 RAS

cal galaxies spanning a much broader range of spectroscopic ages. New CO(1-0) emission line data (estimating the H_2 gas mass) for merger remnants in Paper I are also presented.

In Section 2 we discuss the sample selection, while Section 3 describes new radio observations carried out for some of the galaxies in the present sample. Section 4 presents the results from our analysis. Finally, in Section 5 we summarise our conclusions. Throughout this paper we assume a value $H_0 = 75\,\mathrm{km\,s^{-1}\,Mpc^{-1}}$.

2 THE SAMPLE

One of the difficulties in studying the evolution of ellipticals is ordering them into a time sequence. We address this issue using a new catalogue of spectroscopic galaxy ages recently compiled by Terlevich & Forbes (2001) using a relatively homogeneous dataset of high quality absorption line measurements for galaxies (e.g. Hβ and [MgFe]). The models of Worthey (1994) are applied to this dataset to break the age/metallicity degeneracy providing both age and metallicity estimates for each galaxy. There are several additional caveats regarding the reliability of spectroscopic ages. The uniform assumption of solar element abundance ratios, in particular, is a concern, as are effects from aperture sizes which sample different physical scales, nebular Hβ emission "filling in" the age-sensitive absorption feature, and others. These are all addressed in detail by Terlevich & Forbes (2001), who emphasise that although *absolute* galaxy ages based on spectroscopic techniques are still under debate due to theoretical and observational uncertainties, the ages quoted in their catalogue provide a *relative* time-scale that can be reliably used to order galaxies into an evolutionary sequence. For the purposes of the present investigation the large catalogue of Terlevich & Forbes (2001) provides consistent, and to the extent allowed by the assumptions accurately, derived age-estimates. This is a valuable tool for the purpose of defining an evolutionary sequence, and, despite the concerns in the spectroscopic age derivation, appears at least as effective as alternative methods, and has thus been adopted here.

The present sample comprises all the elliptical galaxies from the Terlevich & Forbes (2001) catalogue with $M_B < -18.5$ mag (total of 79). This absolute magnitude limit is adopted to avoid dwarf systems (total of 10), likely to have different evolutionary histories compared to more massive galaxies.

Additionally, the elliptical galaxy catalogue above is complemented by a sample of 12 merger remnant candidates compiled by Keel & Wu (1995) and comprising systems younger than ≈ 1.5 Gyr. They used morphological and dynamical criteria to assign a dynamical 'stage' number to each system estimating the time since nuclear coalescence. The Keel & Wu sequence is calibrated using spectroscopic age estimates for some of the systems the sample (i.e. NGC 2865, NGC 3921, NGC 7252; Forbes, Ponman & Brown 1998).

The sample used in this study is shown in Table 1, which has the following format:

1. Galaxy name.

2. Heliocentric distance, D, in Mpc, assuming $H_o = 75\,\mathrm{km\,s^{-1}\,Mpc^{-1}}$. No correction for the Local Group velocity or the Virgocentric flow has been applied. These corrections are not expected to modify the estimated distances by more than 10%. Moreover, in our analysis we consider ratios of observed quantities that are independent of distance.

3. Total radio flux density at 1.4 GHz (20 cm; $S_{1.4}^{tot}$) in mJy. For most galaxies in the present sample $S_{1.4}^{tot}$ was obtained from (i) Condon et al. (1991) (ii) the NRAO VLA Sky Survey (NVSS) catalogue (Condon et al. 1998) and (iii) the FIRST survey (Becker, White & Helfand 1995).

4. Spectroscopic galaxy age in Gyr.

5. Far-infrared luminosity in solar units ($L_\odot = 3.83 \times 10^{26}$ W)

$$L_{FIR} = 4\pi\, D^2 \times 1.4 \times S_{FIR}, \qquad (1)$$

where S_{FIR} is the FIR flux in $\mathrm{W\,m^{-2}}$ between 42.5 and 122.5μm (Sanders & Mirabel 1996)

$$S_{FIR}(\mathrm{W\,m^{-2}}) = 1.26 \times 10^{-14} \times (2.58 \times \mathrm{f}_{60} + \mathrm{f}_{100}), \qquad (2)$$

where f_{60} and f_{100} are the IRAS fluxes at 60 and 100μm respectively in Jansky. The scale factor 1.4 in equation (1) is the correction factor required to account principally for the extrapolated flux longward of the IRAS 100μm filter (Sanders & Mirabel 1996).

6. Molecular hydrogen mass, $M(H_2)$, estimated from the CO(1–0) emission. The sources from which the CO(1–0) intensity measurements were obtained are given in Table 1. The conversion factor $N(H_2)/I_{CO} = 3 \times 10^{20}\,\mathrm{cm^{-2}\,(K\,km\,s^{-1})^{-1}}$, appropriate for molecular clouds in the Milky Way (Sanders, Solomon & Scoville 1984) was adopted. It should be noted that use of this conversion factor assumes that the mean properties of the molecular gas in ellipticals and merger remnants (i.e. density, temperature and metallicity) are similar to those of the Milky Way. This effect is discussed in more detail later in the paper. Nevertheless, to facilitate comparison of our results with other studies we use the standard Galactic $N(H_2)/I_{CO}$ conversion factor. In any case the results can be interpreted in terms of CO luminosity (L_{CO}) rather than $M(H_2)$, since a constant scaling factor is used throughout. In case of non-detections, upper limits were calculated by taking the 3σ rms noise per channel multiplied with a standard line-width of $300\,\mathrm{km\,s^{-1}}$ and divided by the number of channels in the adopted velocity interval.

7. Neutral hydrogen mass, $M(HI)$. The H I masses are related to the H I integrated intensities, $F(H\,I)$ (measured in $\mathrm{Jy\,km\,s^{-1}}$), by

$$M(H\,I)(M_\odot) = 2.356 \times 10^5 \times F(H\,I) \times (D/\mathrm{Mpc})^2. \qquad (3)$$

The sources from which the H I intensity measurements were obtained are also given in Table 1. Upper limits are calculated from the equation above by taking the 3σ rms noise and assuming a line-width of $300\,\mathrm{km\,s^{-1}}$. Some ellipticals in our sample have a late type spiral galaxy companion within the H I beam that dominates the observed H I emission. These systems (NGC 4105, NGC 1209, NGC 5638, NGC 7562) are excluded from the statistical analysis of quantities involving H I gas mass and are shown on the plots with different symbols.

8. Total B-band magnitude, B_T. This has been corrected for Galactic extinction, A_B, but not for internal extinction. The A_B values are from Burstein & Heiles (1984).

9. Galaxy X-ray luminosity, L_X, in units of $\mathrm{erg\,s^{-1}}$ from

O'Sullivan, Forbes & Ponman (2000b) scaled to the galaxy distances adopted in the present study.

10. Galaxy environment, field (F), group (G) or cluster (C) from the the catalogues of Tully (1988) and Garcia (1993).

3 OBSERVATIONS

New observations in the ^{12}CO($J = 1-0$) (115 GHz) emission line were carried out in 2000 April using the Onsala Space Observatory (OSO) 20 m telescope. For low declination objects, additional observations in the ^{12}CO($J = 1 - 0$) and ^{12}CO($J = 2 - 1$) (230 GHz) emission lines were performed in 2000 October 10–13 at the Swedish–ESO Submillimeter Telescope (SEST).

The OSO observations were obtained with a single-sideband SIS receiver that operated at a typical system temperature of 450-700 K depending on weather conditions and elevation. The beamwidth and main beam efficiency of the OSO telescope at 115 GHz were 33 arcmin and 0.45 respectively. The spectra were obtained with a 512 × 1 MHz filterbank, yielding a velocity resolution of 2.6 km s^{-1}. A dual beam switch mode with a beam-throw of about 6 arcmin was used to eliminate asymmetries and to produce spectra with flat baselines.

For the SEST observations the SIS 115/230 GHz receiver was employed with two low resolution Acousto Optical Spectrometers (AOS) as backends. The AOS had a bandwidth of 500 MHz for the $J = 1 - 0$ transition yielding a resolution of about 1.8km s^{-1}. For the $J = 2 - 1$ transition the bandwidth was 1000 MHz giving resolution of 0.9 km s^{-1}. Typical system temperatures were about 300 and 200 K for the $J = 1 - 0$ and $J = 2 - 1$ transitions respectively. NGC 2865 was observed in the CO(1–0) emission line only using the SIS 100 GHz receiver because of technical problems with the SIS 115/230 GHz receiver at the time of the observation. The backend was again the low resolution AOS with a bandwidth of 1000 MHz yielding a resolution of about 1.8 km s^{-1}. All observations were made in dual beam switch mode with a beam-throw of 11.2 arcmin. The half power beam sizes and main-beam efficiencies of the SEST are 44 arcsec and 0.70 for the $J = 1-0$ transition and 23 arcsec and 0.50 for the $J = 2 - 1$ transition.

The resulting spectra were reduced using the XSPEC† software. Only first order baselines were subtracted and the resultant spectra were "boxcar" smoothed to a resolution of ≈ 10 or 20 km s^{-1}. Antenna temperatures, T_A^*, were converted to main beam temperatures, T_{mb}, using the relation

$$T_{mb} = T_A^*/\eta_{mb}, \quad (4)$$

where η_{mb} is the main beam efficiency. The spectra of the observed galaxies, in units of main beam temperature are shown in Figure 1, while observational parameters are presented in Table 2. Only one confident detection has been measured, that for the CO(1–0) transition in NGC 2865. The integrated line intensity for this transition $\int T_{mb}\, dv = 0.55$ K km s^{-1}. For the remaining galaxies confident upper limits on $M(H_2)$ can be derived from the non-detections. These upper limits were calculated following the method described in Section 2.

For NGC 6702 there appears to be a statistically significant feature at a velocity which is ≈ 250 km s^{-1} lower than the optical systemic velocity. Wiklind, Combes & Henkel (1995) using data of similar sensitivity do not detect any CO(1–0) emission from this galaxy. If the feature in the NGC 6702 is real it corresponds to an intensity of 0.45K km s^{-1} and a molecular gas mass of $M(H_2) = 3.20 \times 10^8\, M_\odot$. We adopt a conservative approach and assume that no CO(1–0) is detected in this system. More sensitive observations are required to confirm or refute the observed feature.

† http://www.ls.eso.org/lasilla/Telescopes/SEST/handbook/

4 RESULTS

4.1 Star formation

The star-formation activity in galaxies is believed to be tightly associated with the presence of cold gas. Therefore, to better understand the evolution of cold gas in ellipticals, we first explore the evolution of their star-formation activity. Here, we choose to use the 1.4 GHz radio emission as estimator of the galaxy star-formation rate (SFR). The same results and conclusions are obtained if the FIR luminosity is used as a SFR census. It is important to recognise that the 1.4 GHz flux density of radio bright (≈ 1 Jy) ellipticals is dominated by powerful active galactic nuclei (AGN) rather than star-formation. It is still unclear, though, whether the low-level radio emission (at mJy and sub-mJy flux densities) observed in many ellipticals is due to weak AGNs or residual star-formation activity (Wrobel & Heeschen 1991; Ho 1999; Hopkins et al. 2000). Therefore, in the following analysis the radio emission may need to be considered as an upper limit to the SFR of the host galaxy.

We define the ratio, R, between total radio (1.4 GHz) flux density, $S_{1.4}^{total}$ and B-band luminosity (Hummel 1981)

$$R = \log(S_{1.4}^{total}) + 0.4 \times (B_T - 12.5). \quad (5)$$

The R parameter is independent of distance and estimates the ratio between radio power and optical luminosity. It has been demonstrated that the mean radio power is proportional to the mean optical luminosity of galaxies (Hummel 1981). The R parameter also takes into account this effect, providing an estimate of the excess radio emission in galaxies due to star-formation or AGN activity. The R parameter is plotted against the galaxy age in Figure 2.

Galaxies with evidence for strong AGN activity based on either their optical spectroscopic features (Veron-Cetty & Veron 1998) or their radio morphology (e.g. radio lobes; if high resolution radio maps are available) are excluded from subsequent statistical analysis. This ensures that the trends investigated more reliably reflect the evolution of star-formation processes. This piecemeal method for excluding AGN systems is not completely reliable, and a number of the remaining old (> 3 Gyr) ellipticals in the sample have comparatively high radio emission ($R > 1.5$). While the young (< 1 Gyr) post-merger systems with similarly high R values show strong evidence for the presence of starburst activity (Keel & Wu 1995), this is much less typical of evolved elliptical galaxies. The majority of these older systems have

Table 1: The sample

Name	D (Mpc)	$S_{1.4}^{tot}$ (mJy)	Age (Gyr)	L_{FIR} ($10^9 \times L_\odot$)	$M(H_2)^{\mathbf{a}}$ ($10^8 \times M_\odot$)	$M(HI)^{\mathbf{b}}$ ($10^8 \times M_\odot$)	B_T (mag)	$\log L_X$ (erg s^{-1})	Environment
ESO 274-G06	59.4		12.1				13.88		F
ESO 507-G45	61.0	<2.5	17.0				13.60		F
IC 0843	99.9	6.1	17.0	5.8			14.61		G
IC 2006	18.2	<2.5	6.0	0.1	<0.97[6]	2.32[10]	12.21	<41.02	C
IC 3947	76.0	<1.0	17.0				15.45		C
IC 4045	91.9	<1.0	14.4				14.90		C
IC 4051	66.5	<1.0	12.0	<1.5			14.12		C
IC 5105	72.1		17.0	<1.5			12.56		F
IC 5328	41.8		17.0	<0.8	<2.71[6]		12.28		F
IC 5358	115.1	28.3	16.3				13.54	43.6	C
NGC 0315	66.1	772.9	4.9	2.9	<28.1[1]	<13.70[1]	11.94	41.68	G
NGC 0547	73.7	93.1	7.6	<2.7			13.01	40.83	C
NGC 0584	24.7	<2.5	2.1	<0.1		<5.17[3]	11.33	<40.17	G
NGC 0636	24.6	<2.5	3.6	<0.2	<0.63[13]	1.71[2]	12.29	<41.19	G
NGC 0720	22.9	<2.5	3.4	<0.1	<0.65[2]	<1.11[2]	11.16	40.69	G
NGC 0821	23.4	<2.5	7.2	<0.2		<1.04[3]	11.51	<40.41	F
NGC 1209	34.7	14.0	14.8	<0.4		9.93[2]	12.32	<40.78	G
NGC 1339	18.6	<2.5	7.5	<0.1	<1.02[6]		12.51	<40.19	C
NGC 1374	17.3	<2.5	9.8	<0.0			12.00	39.85	C
NGC 1379	17.7	<2.5	7.8	<0.1			11.80	39.22	C
NGC 1399	19.0	209.0	5.0	<0.1		<2.37[3]	10.55	41.67	C
NGC 1404	26.0	4.3	5.0	<0.2			10.97	41.5	C
NGC 1419	28.4	<2.5	8.3	<0.2			13.48	<40.75	C
NGC 1427	18.5	<2.5	6.5	<0.1			11.77	39.87	C
NGC 1453	52.1	28.1	7.6	<1.5		9.59[2]	12.34		G
NGC 1549	16.3		7.6	<0.0			10.72	40.02	G
NGC 1571	59.2		8.9	<0.9			13.23		F
NGC 1600	62.9	62.8	6.9	0.9	<2.58[3]	<23.50[2]	11.85	41.58	F
NGC 1700	51.7	<2.5	2.3	<1.2	<2.05[13]	<16.40[2]	12.09		G
NGC 2329	77.3	670.0	17.0	<2.5			13.14	42.19	C
NGC 2418	67.4		0.9	<2.9	<4.8[13]		13.05		F
NGC 2623	73.8	98.5	0.2	260.0	55.4[9]	18.00[4]	13.91	40.52	G
NGC 2778	27.1	<1.0	8.2	<0.3			13.33	<40.43	G
NGC 2865	35.0	<0.4	1.2	<0.6	1.2[13]	11.00[11]	12.30	<40.44	F
NGC 2911	42.4	58.6	1.2	1.3		19.00[3]	12.42	<40.97	G
NGC 2914	42.0		0.7	<0.9		5.2[12]	14.03		G
NGC 3078	33.3	313.8	13.9			<7.29[3]	11.97	40.72	G
NGC 3377	9.2	<1.0	4.1	0.0		<0.05[3]	11.18	<39.52	G
NGC 3379	11.9	2.7	9.3	<0.0	<0.14[3]	<0.06[3]	10.19	<39.68	G
NGC 3414	18.9	4.0	1.1	<0.3	<0.17[13]	1.00[13]	11.96		G
NGC 3509	102.7	27.9	0.3	36.0		210.00[14]	13.35		?
NGC 3585	18.7	<2.5	3.1	<0.1		<11.90[3]	10.60	39.92	G
NGC 3608	14.8	<1.0	10.0			0.19[4]	11.70	39.76	G
NGC 3818	22.7	<2.5	5.0	<0.2		<1.86[2]	12.56	<40.19	F
NGC 3921	77.8	9.4	0.6	12.8	35.00[10]	51.00[15]	13.06		G
NGC 4105	25.8	5.2	17.0	0.5	<2.51[6]	11.9[8]	11.36	40.53	G
NGC 4194	33.4	102.0	0.1	50.0	12.4[9]	17.1[4]	13.01		F
NGC 4261	29.5	19435.0	9.4	0.2	<5.6[1]	<13.30[2]	11.41	41.15	G
NGC 4278	8.7	518.0	8.4	0.1	<0.31[4]	1.87[5]	10.99	39.82	G
NGC 4339	17.2	<1.0	7.9	<0.1		<0.75[3]	12.26	<39.92	C
NGC 4374	13.3	6495.0	11.0	0.2	<1.14[1]	<1.80[2]	9.97	40.67	C
NGC 4472	11.6	752.0	8.5	<0.1	<0.04[2]	0.27[6]	9.37	41.48	C
NGC 4478	18.4	<1.0	4.1	<0.1		<1.51[3]	12.27	<40.53	C
NGC 4551	19.6	<1.0	5.2	<0.1		0.14[4]	12.82	<39.26	C
NGC 4564	14.8	<1.0	5.9	0.2	<0.87[4]	<0.19[3]	11.97	<39.78	C
NGC 4649	18.8	29.6	10.8	0.6	0.75[5]	4.00[8]	9.77	41.42	C
NGC 4697	16.5	<1.0	8.2	0.3	0.22[3]	<1.73[7]	10.10	40.2	G

Table 1: continued

Name	D (Mpc)	$S_{1.4}^{tot}$ (mJy)	Age (Gyr)	L_{FIR} ($10^9 \times L_\odot$)	$M(H_2)$[a] ($10^8 \times M_\odot$)	$M(HI)$[b] ($10^8 \times M_\odot$)	B_T (mag)	$\log L_X$ (erg s^{-1})	Environment
NGC 4807	92.5	<1.0	5.2	<3.0			14.47		C
NGC 4827	101.3	51.8	10.1				13.90		C
NGC 4840	81.0	<1.0	6.6				14.66		C
NGC 4841	89.4	<1.0	11.6				13.73		C
NGC 4860	106.4	<1.0	11.8	12.5		24.00[8]	14.51		C
NGC 4869	90.5	450.0	14.6				14.72		C
NGC 4872	96.1	<1.0	2.8				15.32		C
NGC 4876	89.0		2.1				15.34		C
NGC 4923	72.1	<1.0	8.5				14.62		C
NGC 4926	105.2	<1.0	13.0	6.1			14.00		C
NGC 4952	78.9	<1.0	6.6	<1.8			13.36		C
NGC 4957	91.7	<1.0	4.9	<2.1			13.98		C
NGC 5018	37.3	3.3	1.5	3.2	<5.25[6]	3.53[3]	11.49	<40.7	G
NGC 5582	19.1	<1.0	17.0	<0.1			12.48	<39.84	F
NGC 5638	24.7	<1.0	7.0	<0.2		4.46[2]	12.10	<40.3	G
NGC 5812	25.3	<2.5	5.0	<0.2		<5.43[3]	11.89	<40.34	F
NGC 5813	25.7	15.8	17.0	<0.2		<0.98[7]	11.30		G
NGC 5831	22.2	<1.0	2.6			<0.63[7]	12.31	<40.21	G
NGC 5846	24.3	22.1	11.7	<0.2	<0.65[7]	3.64[4]	10.91	41.7	G
NGC 6127	61.5	<2.5	9.3	<0.6			13.00	41.35	F
NGC 6702	63.0	27.9	1.9	<6.0	<1.78[8]	<11.80[8]	13.00		F
NGC 6736	57.6		17.0				14.04		F
NGC 6776	73.1		3.2	3.7			12.87	40.82	F
NGC 6868	38.1		17.0	2.2	<2.43[6]	<6.46[3]	11.52	41.31	G
NGC 6958	36.2	16.3	12.1	3.5		<6.55[10]	12.24	<40.7	F
NGC 7052	62.5	162.1	10.5	5.3	<2.2[8]	<6.30[9]	12.81		F
NGC 7252	62.5	25.3	1.0	37.0	36.07[11]	35.00[15]	12.54	40.65	G
NGC 7454	26.5	<2.5	5.2	<0.4			12.55	<40.27	G
NGC 7562	46.9	<2.5	11.0	<1.3		23.00[4]	12.41	<41.06	G
NGC 7585	46.0		1.4	0.7	<1.64[13]	<670[16]	12.22		F
NGC 7619	50.0	21.1	9.0	<1.3		<3.71[7]	11.94	41.82	G
NGC 7626	45.4	700.0	12.2	<0.8		<3.06[3]	12.00	41.17	C
NGC 7727	24.7	3.4	1.3	0.6	1.00[12]	5.00[3]	11.41		G
NGC 7785	51.0	34.3	8.3	<0.8		<3.86[7]	12.46		F

[a]**CO references**

1: Elfhag et al. 1996; 2: Braine Henkel & Wiklind 1997; 3: Sofue et al 1993; 4: Bregman Hogg & Roberts 1992; 5: Sage & Wrobel 1989; 6: Huchtmeier & Tammann 1992; 7: Huchtmeier et al. 1988; 8: Wiklind, Combes & Henkel 1995; 9: Sanders et al. 1991; 10: Yun & Hibbard 1999; 11: Andreani et al. 1995; 12: Crabtree et al. 1994; 13: present study

[b]**H I references**

1: Chamaraux, Balkowski & Fontanelli 1987; 2: Huchtmeier 1994; 3: Roberts et al. 1991; 4: Bottinelli et al. 1990; 5: Burstein, Krumm & Salpeter 1987; 6: McNamara et al. 1994; 7: Knapp, Turner & Cunniffe 1985; 8: Huchtmeier, Sage & Henkel 1995; 9: Wiklind, Combes & Henkel 1995; 10: Martin1998; 11: Schiminovich et al. 1994; 12: Bottinelli et al. 1980; 13: Huchtmeier 1997; 14: Heckman et al. 1983; 15: Hibbard & van Gorkom 1996; 16: Eskridge et al. 1991

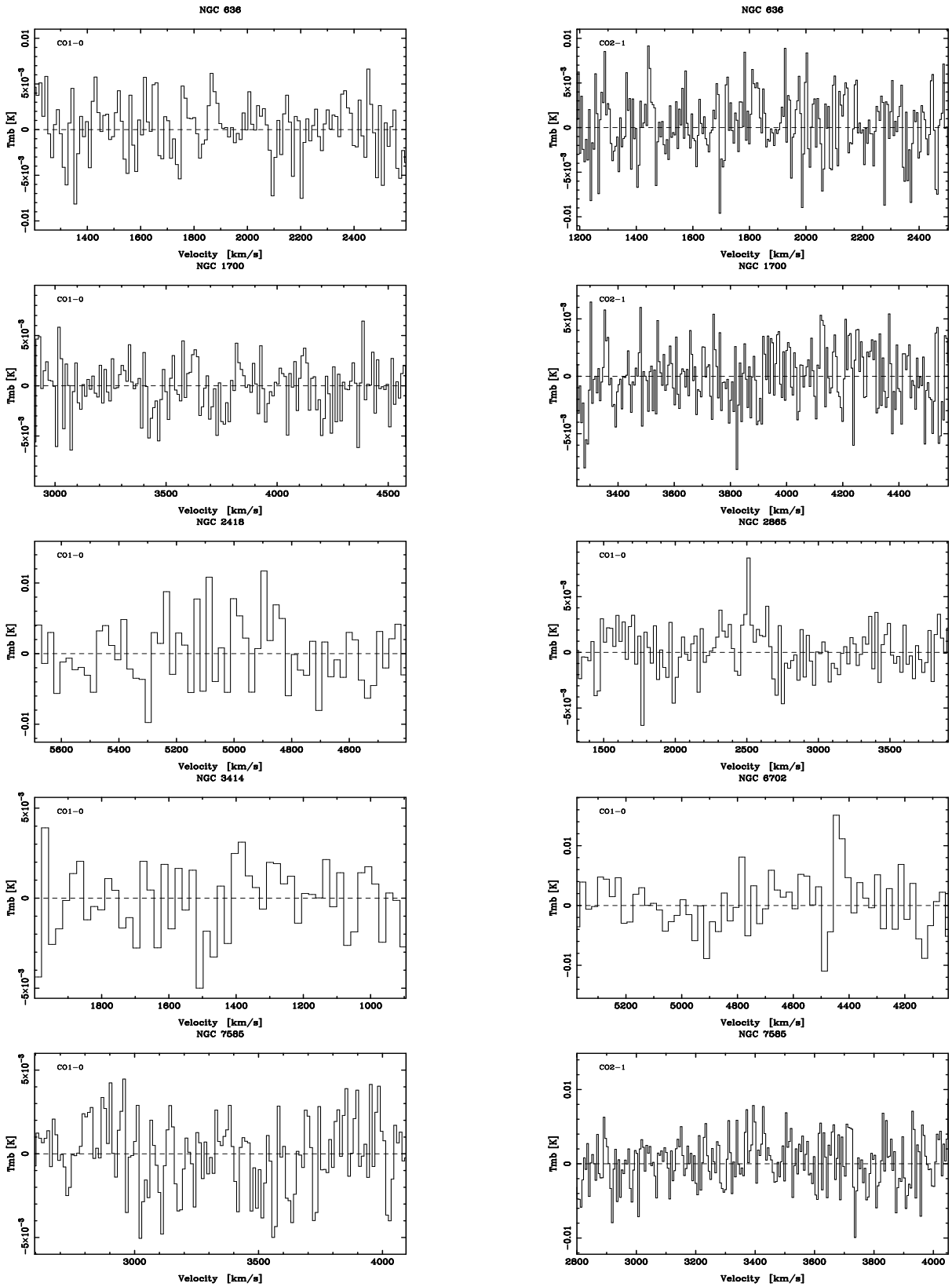

Figure 1. Spectra of the observed galaxies. The channel-to-channel velocity resolutions are the same as those given in Table 2. Galaxies NGC 636, NGC 1700, NGC 2865 and NGC 7585 were observed with the SEST. NGC 2418, NGC 3414 and NGC 6702 were observed with the OSO 20 m telescope

Table 2. Observational parameters

Galaxy Name	RA (J2000)			DEC (J2000)			$v^{(a)}$ (km s^{-1})	CO(1–0) $\delta T_{mb}^{(b)}$ (mk)	CO(1–0) $\delta v^{(c)}$ (km s^{-1})	CO(2-1) $\delta T_{mb}^{(b)}$ (mk)	CO(2-1) $\delta v^{(c)}$ (km s^{-1})	Telescope
NGC 0636	01	39	06.5	-07	30	46	1847	3.2	10.9	3.6	5.5	SEST
NGC 1700	04	56	56.2	-04	51	56	3915	2.5	10.9	2.6	5.5	SEST
NGC 2418	07	36	37.5	17	53	02.3	5057	4.6	21.2	-	-	OSO
NGC 2865	09	23	30.1	-23	09	43	2611	2.0	21.8	-	-	SEST
NGC 3414	10	51	16.3	27	58	28.4	1434	2.1	20.9	-	-	OSO
NGC 6702	18	46	57.6	45	42	19.8	4712	4.8	20.8	-	-	OSO
NGC 7585	11	18	25.4	58	47	10.7	1787	2.8	10.9	3.3	5.5	SEST

(a) optical velocity
(b) Channel–to–channel noise rms
(c) Channel width used to derive rms and to plot spectra

radio flux densities at the 1 Jy level and are likely to belong to the "classic" AGN radio population, although in the absence of unambiguous spectroscopic or morphological classification, they have been retained in the following analysis.

With these caveats in mind, and despite the many non-detections, there is evidence for a decline in the star-formation rates (traced by radio emission) from early merger-remnants to old ellipticals. This can be demonstrated by estimating the mean R parameter within different age bins using survival analysis techniques implemented in the ASURV package (LaValley, Isobe & Feigelson 1992; Isobe, Feigelson & Nelson 1986). Because of the many upper limits, and the probable (albeit unintentional) inclusion of several AGN systems, the mean R values in the last three bins are likely to be overestimates of the level of star-formation present. This reinforces the suggestion that the intensity of star-formation processes decreases with galaxy age.

Also shown in Figure 2 are simple models that assume that the galaxy SFR follows an exponential decay of the form

$$SFR \propto e^{-t/\tau}, \tag{6}$$

where t is the time since the onset of the star-formation and τ is the e-folding parameter. For this SFR law the population synthesis code of Bruzual & Charlot (1993) with a Salpeter IMF is used to predict the galaxy B-band luminosity evolution. Additionally, to estimate the 1.4 GHz radio luminosity ($L_{1.4}$), we assume that $L_{1.4}$ is directly proportional to the model galaxy SFR. Following Condon (1992) and assuming a Salpeter IMF we find

$$L_{1.4} = SFR \times 8.6 \times 10^{20}\,(\mathrm{W\,Hz^{-1}}), \tag{7}$$

where the SFR is estimated from equation 6. Models with e-folding parameter $\tau \approx 2 \times 10^8 - 1 \times 10^9$ yrs can reproduce the observed range of radio emission, with the exception of powerful radio ellipticals, dominated by AGNs. It should be noted that our aim is not to find the best fit to the observed trend but to demonstrate that simple models assuming a burst of star-formation that declines with time can reproduce both the observed trend and the the range of R parameters from early merger-remnants to evolved ellipticals. Indeed, the adopted model does not include important processes such as recycling and heating of the gas. Additionally, the radio emission of some ellipticals in the present sample are likely to be dominated by AGNs rather than SFR. Consequently, the adopted model with $\tau \approx 2 \times 10^8 - 1 \times 10^9$ yrs is likely to represent a lower envelope. Moreover, the spectroscopic ages for the galaxies in the present sample assume an instantaneous burst of star-formation rather than a continuous decline. Estimating spectroscopic ages using models with finite bursts of star-formation will result in older galaxy ages than the ones estimated here. The SFR in the Bruzual & Charlot models, however, declines fast enough that any differences should be small for old systems (e.g. $> 3-4$ Gyr).

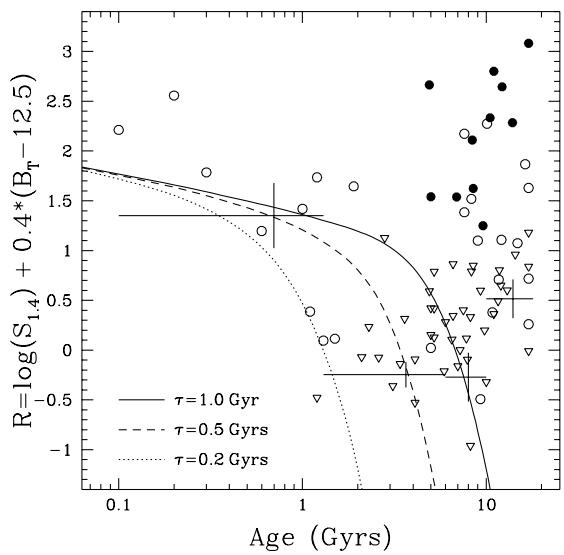

Figure 2. Total radio to B-band flux ratio ($R = \log S_{1.4}^{tot} + 0.4 \times [B_T - 12.5]$) as a function of galaxy age. Open circles are detections while triangles represent upper limits. Filled circles are ellipticals with radio morphology or optical spectroscopic features indicative of powerful AGN activity. The crosses signify the mean R for ellipticals averaged within age bins. The horizontal error bars represent the width of the bin and the vertical error bars are the standard error on the mean. The curves are the models described in the text.

We further explore the star-formation activity in ellipticals using the ratio of FIR luminosity to molecular hydrogen mass $L_{FIR}/M(H_2)$. This estimates the number of massive stars formed per molecular cloud and is thus, related to the integrated galaxy star-formation efficiency (SFE). Figure 3

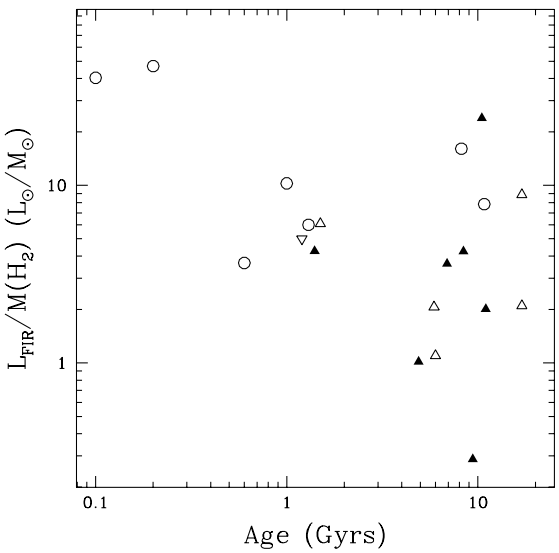

Figure 3. Star-formation efficiency ($L_{FIR}/M(H_2)$) as a function of galaxy age. Open circles are detections while triangles represent upper and lower limits. Filled symbols are ellipticals with radio morphology or optical spectroscopic features indicative of powerful AGN activity.

plots the SFE as a function of the age for the galaxies in the present sample. There is significant scatter, especially for old systems, and many lower limits due to uncertain $M(H_2)$ estimates. Excluding AGNs, the Kendal tau test gives a probability of 78% that no correlation is present, suggesting that the SFE of ellipticals and merger remnants is roughly constant with time. There is only tenuous evidence for a decline in the case of early merger remnants and young ellipticals for ages < 2 Gyr.

Therefore, although we find evidence that the SFR of ellipticals is declining the efficiency of the star-formation appears to remain unchanged with age, with the possible exception of very young merger remnants. This is in agreement with studies of the SFE variations among early type galaxies (Lees et al. 1991). It has been suggested, however, that the FIR luminosity of evolved ellipticals originates from cold rather than warm dust, and thus it is not a good estimator of the low-level SFR in these systems (Lees et al. 1991). Similarly, it has been proposed that the FIR luminosity of ellipticals is not sensitive to on-going star-formation but depends on both the mass-loss rate of evolved stars and the mass of the hot X-ray emitting gas (e.g. Bregman, Hogg & Roberts 1992). In any case, more data, both FIR luminosities and $M(H_2)$ estimates, are required to further constrain the SFE of elliptical galaxies.

4.2 Cold gas evolution

The ratio of cold gas mass (molecular and neutral hydrogen) to B-band luminosity ($[M(HI)+M(H_2)]/L_B$) is plotted against spectroscopic galaxy age in Figure 4. Assuming that L_B provides, to a first approximation, a measure of the total galaxy mass, the ratio $[M(HI)+M(H_2)]/L_B$ estimates the fraction of cold gas mass in the system. It is clear that this quantity decreases from early merger remnants to young ellipticals on a time scale of 1–2 Gyr, as shown in Paper I. This is supported by the generalised Kendal tau and the Spearman rho tests, which indicate a strong anticorrelation between age and cold gas fraction at a significance level of 99.99%. This result is dominated by the gas rich young merger remnants. Applying these statistical tests only to the sub-sample of old (> 1.5 Gyr) ellipticals, we find weak or no correlations between cold gas content and spectroscopic age. This suggests little further decline in cold gas fraction after the initial sharp decrease.

In the context of the merger scenario for the formation of ellipticals, this result is consistent with major changes in the cold gas content of these systems due to depletion by star-formation, for example, occuring predominantly by 1–2 Gyr after the merger event, with a roughly constant fraction of cold gas remaining during subsequent evolution. If there is quiescent low-level star-formation, which would be expected to continue to steadily reduce the cold-gas fraction, the latter effect might be explained as a "steady-state" scenario, either due to (i) injection of cold gas from mass shed by evolved stars (Faber & Gallagher 1976), (ii) fading of the stellar population with age resulting in a decrease in L_B, (iii) the return of the H I expelled into tidal tails during early stages of the interaction (Hibbard & van Gorkom 1996). Alternatively, it is possible that the mechanism responsible for the initial depletion of the gas (e.g. SFR) declines rapidly with time and hence, does not have any significant effect on the remaining cold gas reservoirs for ages >1–2 Gyr. Nevertheless, despite the scatter in Figure 4, there may be a hint of a slow decline in cold gas fraction for evolved systems suggested by the decreasing mean within the age bins shown, although this effect is small enough that it may simply be an artifact of the scatter.

It should be noted that the present study assumes a standard CO–to–H_2 conversion factor, $N(H_2)/I_{CO} = 3 \times 10^{20}\,\mathrm{cm}^{-2}\,(\mathrm{K\,km\,s}^{-1})^{-1}$, appropriate for molecular clouds in the Milky Way (Sanders, Solomon & Scoville 1984). The molecular clouds in ellipticals and merger remnants, though, might have properties (i.e. density and temperature) different to those of the Milky Way. Such differences are expected to modify the CO–to–H_2 conversion factor. Therefore, it is possible that the declining trend between merger remnants and evolved ellipticals in Figure 4 might be due to systematic variations in the $N(H_2)/I_{CO}$ factor between young merger remnants and evolved ellipticals. In particular, the $N(H_2)/I_{CO}$ factor has been shown to depend on the mean temperature ($< T >$) and density ($< \rho >$) of the intergalactic medium according to the relation (Maloney & Black 1988)

$$N(H_2)/I_{CO} \propto < \rho >^{1/2} < T >^{-1} . \quad (8)$$

It is clear that if the mean molecular gas temperature in evolved ellipticals is lower than that in early merger remnants, due to lower levels of star-formation heating up the clouds, then use of the same conversion factor will systematically underestimate $M(H_2)$ in old ellipticals. On the contrary, the higher molecular gas densities expected in merger remnants due to compression have the opposite effect on the conversion factor. Therefore, if temperature variations are to explain the observed trend in Figure 4, large differences, by as much as 1.5 dex, are required. Moreover, high

molecular gas temperatures are usually associated with enhanced H_2 mean densities. Consequently, variations of the $N(H_2)/I_{CO}$ factor alone cannot easily explain the observed trend in Figure 4.

The CO–to–H_2 conversion factor is also sensitive to the metallicity, Z, of the galaxy. In particular, Arnault et al. (1998) suggest that the $N(H_2)/I_{CO}$ varies with $Z^{-2.2}$. Therefore, if metallicity variations are to explain the trend in Figure 4 (1.5 dex decline) then young merger remnants should be as much as ≈ 5 times more metal rich than evolved ellipticals. Indeed, a higher than solar metallicity translates to a lower $N(H_2)/I_{CO}$ factor compared to the Galactic one and hence, $M(H_2)$ is overestimated when using the standard Galactic conversion factor. Such a large metallicity excess from merger remnants to evolved ellipticals would be difficult to explain.

Also shown in Figure 4 are the predictions of the simple model described in the previous section. In this model the cold gas mass, M_g, is assumed to be the mass fraction of the galaxy that remains to be used for star-formation (i.e. the mass of the galaxy not in stars). It can be shown that for an exponential SFR the gas mass decreases according to the relation

$$M_g \propto e^{-t/\tau}. \quad (9)$$

This model with the *same* parameters as used in the previous section, $\tau \approx 2 \times 10^8 - 1 \times 10^9$, reproduces the observed trend from early merger remnants to evolved ellipticals reasonably well, at least for ages < 7 Gyr. On the contrary, older systems are gas rich compared to the model prediction. This suggests that cold gas depletion due to on-going star-formation is, at least partially, a plausible mechanism for the observed trend in Figure 4.

Previous studies of the cold gas content of merger remnants show that these systems are gas rich compared to evolved ellipticals and S0s (Hibbard et al. 1994; Paper I). To resolve this problem Hibbard et al. (1994) suggested that low level residual SFR could further deplete the gas reservoirs of these systems within few Gyr to values typical to E/S0s. Clearly the trend in Figure 4 is consistent with this scenario.

Figure 5 plots the H I mass fraction as a function of spectroscopic galaxy age. As with the cold gas fraction in Figure 4, it is clear that $M(\mathrm{H\,I})/\mathrm{L_B}$ also decreases, on average, from young merger remnants to evolved ellipticals. This supports our conclusions drawn from the trends explored in Figure 4, suggesting they are unlikely to be artifacts of the adopted CO–to–H_2 conversion factor. For Figure 5 the generalised Kendal tau and the Spearman rho tests again indicate a strong anticorrelation between age and H I gas fraction at a significance level of 99.99%, a result dominated by the young merger remnants. For older systems (> 1.5 Gyr), there is again no statistically significant trend with age, although the decline in the mean from the second bin to the third is still suggestive.

Sansom et al. (2000) also studied the $M(H\,I)/L_B$ evolution of ellipticals using the fine-structure index, Σ, to quantify morphological peculiarities in the light profile of the galaxies and to order them into an evolutionary sequence. They find no evidence of a decrease in the cold gas along their evolutionary sequence for their sample, which includes only 2 merger remnants and is dominated by older systems

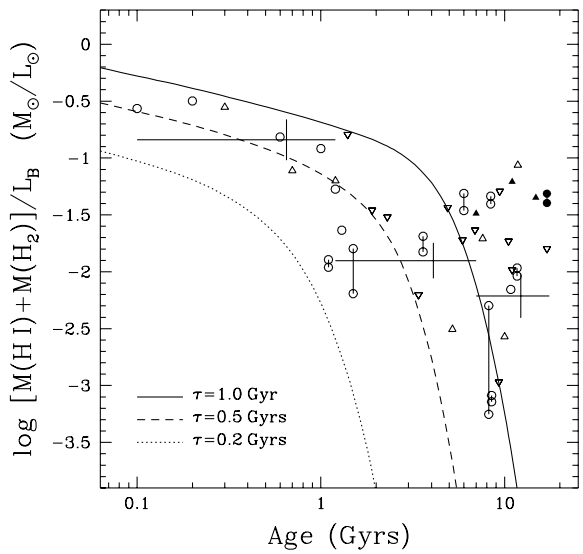

Figure 4. Total mass of neutral and molecular hydrogen normalised to the B-band luminosity as a function of galaxy age. Circles are detections while triangles represent upper or lower limits. Points connected with a line represent the upper and lower $[M(H_2) + M(HI)]/L_B$ limits for that system. Filled symbols are for ellipticals with nearby late type galaxy companions that dominate the observed H I emission (NGC 4105, NGC 1209, NGC 5638, NGC 7562; section 2), which are excluded from the analysis. The crosses signify the mean cold gas content for ellipticals averaged within age bins. The horizontal error bars represent the width of the bin and the vertical error bars are the standard error on the mean. The curves are the models described in the text. There is evidence for a decrease in $[M(H_2) + M(HI)]/L_B$ from early merger-remnants to old ellipticals indicating cold gas depletion.

(> 1.5 Gyr). This is consistent with the trend seen in our sample over this age range.

Finally, we explore whether net conversion of atomic to molecular hydrogen is occurring in ellipticals. In particular, in the merger picture for elliptical galaxy formation, the gravitational instabilities experienced during the interaction can force about half of the outer disc H I into a tail, the rest of the H I being forced into the inner regions (Hibbard & Mihos 1995). Hibbard & Van Gorkom (1996), however, found little evidence for neutral hydrogen within remnant bodies, with most of it lying in the outer regions (i.e. tidal features). One of the proposed mechanisms to resolve this discrepancy is net conversion from H I to H_2. Figure 6 plots the ratio of neutral to molecular hydrogen mass as a function of spectroscopic galaxy age. Despite the limited data available there is some evidence for a correlation, suggesting that net H I to H_2 conversion might be taking place. The generalised Kendall tau test indicates a correlation, albeit at the 2.5σ significance level. This is primarily driven by the NGC 2623 which has the lowest H I/H_2 ratio in the sample. Excluding this galaxy from the analysis, the Kendall tau test finds no significant correlation between age and H I/H_2 ratio (probability of a correlation $\approx 70\%$). Therefore, we conclude that any net H I to H_2 conversion is small. Similarly, searches for molecular hydrogen in the merger remnants NGC 7252

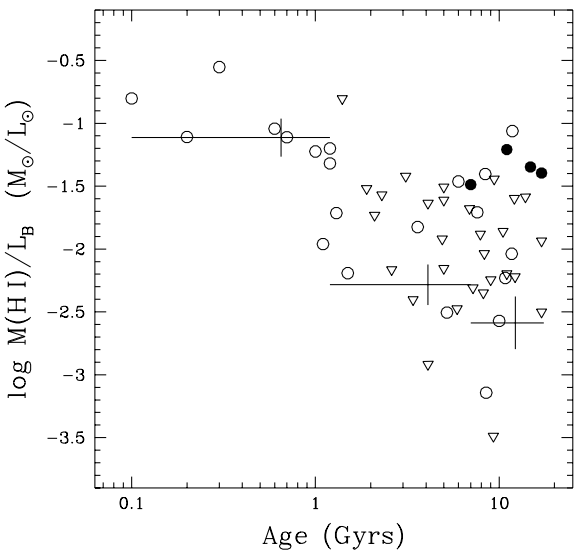

Figure 5. Mass of neutral hydrogen normalised to B-band luminosity as a function of galaxy age. Circles are detections while triangles represent upper or lower limits. Filled symbols are for ellipticals with nearby late type galaxy companions that dominate the observed H I emission (NGC 4105, NGC 1209, NGC 5638, NGC 7562; section 2), which are excluded from the analysis. The crosses signify the mean H I content for ellipticals averaged within age bins. The horizontal error bars represent the width of the bin and the vertical error bars are the standard error on the mean. There is evidence for a decrease in $M(HI)/L_B$ from early merger-remnants to old ellipticals indicating gas depletion.

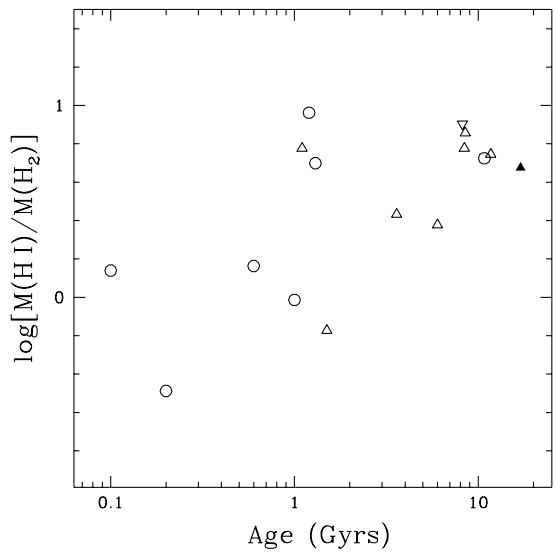

Figure 6. Neutral to molecular hydrogen mass, $M(HI)/M(H_2)$, as a function of galaxy age. Filled symbols are for elliptical galaxies with nearby late type galaxy companions that dominate the observed H I emission (section 2), which are excluded from the analysis. There is no obvious trend, implying little net conversion from H I to H_2 during the interaction.

and NGC 3921 have revealed that these systems have below average molecular gas content compared with their spiral progenitors (Solomon & Sage 1988; Young & Knezek 1989; Hibbard & van Gorkom 1996). This suggests that any net conversion of atomic to molecular hydrogen is relatively inefficient, in agreement with our results.

5 CONCLUSIONS

In this paper we study the cold gas evolution of early type galaxies and merger remnants. Spectroscopic ages, estimating the time since the last major starburst event, are used to order the galaxies in the present sample into an evolutionary sequence. We find strong evidence for a decrease of the cold gas mass fraction (H I and H_2) from early merger remnants to evolved ellipticals. The observed cold gas decline is predominantly occuring 1–2 Gyr after the merger event, and the cold gas fraction remains essentially constant thereafter. Simple models involving on-going but declining star-formation activity provide a plausible explanation for the observed trend. This is consistent with the "merger hypothesis", where the interaction induced starburst is depleting the cold gas reservoirs of the system to values typical for those of evolved ellipticals. We also find little evidence for net conversion of H I to H_2 in merger remnants and ellipticals, particularly for ages > 1 Gyr, in agreement with previous studies.

6 ACKNOWLEDGEMENTS

We wish to thank an anonymous referee for several very constructive and helpful comments. AMH acknowledges support from NASA LTSA grant NRA-98-03-LTSA-039. This research has made use of the NASA/IPAC Extragalactic Database (NED), which is operated by the Jet Propulsion Laboratory, Caltech, under contract with the National Aeronautics and Space Administration.

REFERENCES

Andreani P., Casoli F., Gerin M., 1995, A&A, 300, 43
Arnault P., Kunth D., Casoli F., Combes F., 1988, A&A,205, 41
Barnes J. E., 1988, ApJ, 331, 699
Barnes J. E., 1992, ApJ, 393, 484
Becker R. H., White R. L., Helfand D. J., 1995, ApJ, 450, 559
Bottinelli L., Gouguenheim L., Paturel G., 1980, A&A, 88, 32
Bottinelli L., Gouguenheim L., Fouque P., Paturel G., 1990, A&AS, 82, 391
Braine J., Henkel C., Wiklind T., 1997, A&A, 321, 765
Bregman J. N., Hogg D. E., Roberts M. S., 1992, ApJ, 387, 484
Brodie J. P., Schroder L. L., Huchra J. P., Phillips A. C., Kissler-Patig M., Forbes D. A., 1998, AJ, 116, 691
Brown B. A., Bregman J. N., 2000, ApJ, 539, 592
Bruzual A. G., Charlot S., 1993, ApJ, 405, 538
Burstein D., Krumm N., Salpeter E. E., 1987, AJ, 94, 883
Burstein D., Heiles C., 1984, ApJS, 54, 33
Casoli F., Dupraz C., Combes F., Kazes I., 1991, A&A, 251, 32
Chamaraux P., Balkowski C., Fontanelli P., 1987, A&AS, 69, 263
Ciotti L., D'Ercole A., Pelegrini S., Renzini A., 1991, ApJ, 376, 380
Condon J. J., 1992, ARA&A, 30, 575
Condon, J. J., Cotton, W. D., Greisen, E. W., Yin, Q. F., Perley, R. A., Taylor, G. B., & Broderick, J. J. 1998, AJ, 115, 1693

Condon J. J., Huang Z. P., Yin Q. F., Thuan T. X., 1991, ApJ, 378, 65
Crabtree D. R., Smecker-Hane T., 1994, AAS, 185, 107.14
Elfhag T., Booth R. S., Hoeglund B., Johansson L. E. B., Sandqvist A., 1996, A&AS, 115, 439
Eskridge P. B., Pogge R. W., 1991, AJ, 101, 2056
Fabbiano G., 1989, ARA&A, 27, 87
Faber S. M., Gallagher J. S., 1976, ApJ, 204, 365
Forbes D. A., Brodie J. P., Grillmair C. J., 1997, AJ, 113, 1652
Forbes D. A., Ponman T. J., Brown R. J. N., 1998, 508, L43
Garcia A. M., 1993, A&AS, 100, 47
Georgakakis A., Forbes D. A., Norris R. P., 2000, MNRAS, 318, 124; Paper I
Heckman T. M., Balick B., van Breugel W. J. W., Miley G. K., 1983, AJ, 88, 583
Hibbard J. E., Guhathakurta P., van Gorkom J. H., Schweizer F., 1994, AJ, 107, 67
Hibbard J. E., Mihos J. C., 1995, AJ, 110, 140
Hibbard J. E., van Gorkom J. H., AJ, 1996, 111, 655
Ho L. C., 1999, ApJ, 510, 631
Hopkins A., Georgakakis A., Cram L., Afonso J., Mobasher B., 2000, ApJS, 128, 469
Hummel E., 1981, A&A, 96, 111
Huchtmeier W. K., Bregman J. N., Hogg D. E., Roberts M. S., 1988, A&A, 198L, 17
Huchtmeier W. K., Sage L. J., Henkel C., 1995, A&A, 300, 675
Huchtmeier W. K., 1994, A&A, 286, 389
Huchtmeier W. K., Tammann G. A., 1992, A&A, 257, 455
Huchtmeier W. K., 1997, A&A, 319, 401
Isobe T., Feigelson E. D., Nelson P. I., 1986, ApJ, 306, 490
James P., Bate C., Wells M., Wright G., Doyon R., 1999, MNRAS, 309, 585
Joseph R. D., Wright G. S., 1985, MNRAS, 214, 87
Keel W. C., Wu W., 1995, AJ, 110, 129
Knapp G. R., Turner E. L., Cunniffe P. E., 1985, AJ, 90, 454
LaValley M., Isobe T., Feigelson E. D., 1992, BAAS, 24, 839
Lees J. F., Knapp G. R., Rupen M. P., Phillips T. G., 1991, ApJ, 379, 177
Malin D. F., Carter D., 1980, Nature, 285, 643
Martin M. C., 1998, A&AS, 131, 77
McNamara B. R., Sancisi R., Henning P. A., Junor W., 1994, AJ, 108, 844
Miller B. W., Whitmore B. C., Schweizer F., Fall S. M., 1997, AJ, 114, 2381
O'Sullivan, Forbes D. A., Ponman T. J., 2000a, MNRAS, in press
O'Sullivan, Forbes D. A., Ponman T. J., 2000b, in preparation
Roberts M., Hogg D., Bregman J. N., Forman W. R., Jones C., 1991, ApJS, 75, 751
Sage L. J., Wrobel J. M., 1989, ApJ, 344, 204
Sanders D. B., Scoviller N. Z., Soifer B. T., 1991, ApJ, 370, 158
Sanders D. B., Solomon P. M., Scoville N. Z., 1984, ApJ, 276, 182
Sanders D. B., Mirabel I. F., 1996, ARA&A, 34, 749
Sansom A. E., Hibbard J. E., Schweizer F., 2000, AJ, 120, 1946
Schiminovich D., van Gorkom J. H., van der Hulst J. M., Kasow S., 1994, ApJ, 423, L101
Schweizer W., 1996, AJ, 111, 109
Schweizer W., Seitzer P., 1988, ApJ, 328, 88
Sofue Y. & Wakamatsu K., 1993, PASJ, 45, 529
Solomon P. M., Sage L. J., 1988, ApJ, 334, 613
Terlevich A. I., Forbes D. A., 2001, MNRAS, submitted
Toomre A., Toomre J., 1972, ApJ, 178, 623
Tully R. B., 1988, *Neabry Galaxies Catalogue*, Cambridge University Press
van den Bergh S., 1984, PASP, 96, 329
Veron-Cety M., Veron P., 1996, ESO Scientific report No. 17, A Catalogue of Quasars and Active Nuclei, Tth edition
White R. E. I., Sarazin C. L., 1991, ApJ, 367, 476
Whitmore B. C., Schweizer F., 1995, AJ, 109, 960
Wiklind T., Combes F., Henkel C., 1995, A&A, 297, 643
Worthey G., 1994, ApJS, 95, 107
Wrobel J. M., & Heeschen D. S., 1991, AJ, 101, 148
Young J. S., Knezek P. M., 1989, ApJ, 347, L55
Yun M. S., Hibbrand J. E., 1999, astro-ph/9903463
Zepf S. E., Ashman K. M., English J., Freeman K. C., Sharples R. M., 1999, AJ, 1999, 118, 752